3418 *Chem. Mater.* **2010,** *22,* 3418–3425
DOI:10.1021/cm100408y

CHEMISTRY OF MATERIALS
Article

Nanometer Scale Proton Conductivity and Dynamics of $CsHSO_4$ and $H_3PW_{12}O_{40}$ Composites under Non-Humidified Conditions

Yusuke Daiko,*[,†] Shigenobu Hayashi,[‡] and Atsunori Matsuda*[,§]

[†]*Department of Materials Science and Chemistry, University of Hyogo, Shosha, Himeji, Hyogo 671-2201, Japan,* [‡]*Research Institute of Instrumentation Frontier, National Institute of Advanced Industrial Science and Technology (AIST), Tsukuba Central 5, 1-1-1 Higashi, Tsukuba, Ibaraki 305-8565, Japan, and* [§]*Department of Electrical and Electronic Information Engineering, Toyohashi University of Technology, Tempaku-cho, Toyohashi, Aichi 441-8580, Japan*

Received February 9, 2010. Revised Manuscript Received April 20, 2010

We prepared composites of $CsHSO_4$ and $H_3PW_{12}O_{40}\cdot 6H_2O$ (WPA-$6H_2O$), $x CsHSO_4\cdot(100-x)$-WPA-$6H_2O$ (mol %) by mechanical milling (MM). The nanometer scale proton dynamics and the non-humidified proton conductivity were investigated using ^1H nuclear magnetic resonance (NMR) and alternating current impedance spectroscopies. The non-humidified proton conductivities at 100 °C for pure $CsHSO_4$ and WPA-$6H_2O$ were 4.0×10^{-7} and 1.0×10^{-7} S/cm, respectively. On the other hand, the proton conductivity increased significantly to approximately 3×10^{-3} S/cm for the $x = 80$ and $x = 90$ composites. Proton conductivity, ^1H spin−lattice relaxation time (T_1) and theoretical calculation results suggested the formation of a *reacted region* with high proton conductivity around the WPA-$6H_2O$ cluster after the MM. T_1 measurements for the $90CsHSO_4\cdot 10$WPA-$6H_2O$ (mol %) composite revealed that there were two relaxation components, and that the long T_1 and short T_1 components could be correlated to proton motion inside the WPA-$6H_2O$ cluster and inside the reacted region, respectively. From an analysis of the short T_1, we found that the proton jumping rate at 100 °C of $CsHSO_4$ increased approximately 1,600 times after mixing $CsHSO_4$ and WPA-$6H_2O$. The proton conductivity of the reacted region was estimated to be 10×10^{-3} S/cm from a theoretical calculation using the effective medium theory.

1. Introduction

Conductors with high proton conductivity at higher than 100 °C in a dry atmosphere have attracted considerable attention because of their potential application as gas sensors and fuel cells. Fuel cell operation under high temperature and dry conditions is desired to improve the CO tolerance of Pt electrodes, increase the reaction rate, manage water more efficiently, and simplify system integration.[1,2]

Inorganic solid acids such as $MeHAO_4$ and $Me_3H(AO_4)_2$ (Me = Rb, Cs, NH_4, A = S, Se) have been widely studied because of their high proton conductivity, even under dry conditions. These solid acids show characteristic phase transition behavior. For example, the crystal structure of $CsHSO_4$ is monoclinic with a space group of $P2_1/c$ around room temperature. When the temperature increases above the phase transition temperature (Tg = 144 °C), the crystal structure becomes tetragonal with a space group of $I4_1/amd$, and $CsHSO_4$ exhibits high proton conductivity (superprotonic phase transition).

These solid acids were first studied in the 1950s because of their good ferroelectric and ferroelastic properties.[3,4] In 1981, it was reported that the dielectric constants (ε' and ε'') of $CsHSO_4$[5] and $CsHSeO_4$[6] changed significantly by the phase transition. Itoh et al. studied the crystal structure of $CsHSO_4$ by X-ray diffraction.[7] They found that only two of the four oxygen atoms (from SO_4 tetrahedra) per molecule participate in the formation of hydrogen bonds. This suggests that $CsHSO_4$ has disordered H atoms. In 1982 Baranov et al. first reported the relationship between the phase transitions and proton conductivity of $CsHSO_4$.[8]

The structural mechanisms of the "*superprotonic phase transition*" have been studied by high resolution neutron powder diffraction using deuterated $CsDSO_4$.[9] It was revealed that the hydrogen bond networks become disordered

*To whom correspondence should be addressed. E-mail: daiko@u-hyogo.ac.jp (Y.D.) matsuda@ee.tut.ac.jp (A.M.). Fax: +81 79 267-4722 (Y.D.), +81 532 44-6799 (A.M.).

(1) Li, Q.; He, R.; Jensen, J. O.; Bjerrum, N. J. *Chem. Mater.* **2003**, *15*, 4896–4915.
(2) Steele, B. H.; Heinzel, A. *Nature* **2001**, *414*, 345–352.
(3) Matthias, B. T.; Remeika, J, P. *Phys. Rev.* **1956**, *103*, 262–262.
(4) Pepinsky, R.; Vedam, K.; Hoshino, S.; Okaya, Y. *Phys. Rev.* **1958**, *111*, 1508–1510.
(5) Komukae, M.; Osaka, T.; Makita, Y.; Ozaki, T.; Itoh, K.; Nakamura, E. *J. Phys. Soc. Jpn.* **1981**, *50*, 3187–3188.
(6) Wolak, J.; Czapla, Z. *Phys. Status Solidi A* **1981**, *67*, K171–K174.
(7) Itoh, K.; Ozaki, T.; Nakamura, E. *Acta Crystallogr.* **1981**, *B37*, 1908–1909.
(8) Baranov, A. I.; Shuvalov, L. A.; Shchagina, N. M. *JETP Lett.* **1982**, *36*, 459–462.
(9) Belushkin, A. V.; David, W. I. F.; Ibberson, R. M.; Shuvalov, L. A. *Acta Crystallogr.* **1991**, *B47*, 161–166.

Published on Web 05/04/2010

and that unoccupied proton locations may allow proton hopping. Many articles that describe the proton conductivity of $CsHSO_4$ and $CsDSO_4$ have also been published.[10−12] It was established that deuteration has practically no effect on the superprotonic phase transition temperature.

The diffusion of protons in the superprotonic phase of $CsHSO_4$ was also studied by quasielastic neutron scattering.[13] It was suggested that the long-range proton transfer in the superprotonic phase consists of two stages; the first is the displacement of a proton along the hydrogen bond and the second is the reorientation of the SO_4 tetrahedra. A molecular dynamic (MD) simulation of $CsDSO_4$ has been performed to validate the results from neutron powder diffraction.[14] It is worth noting that this proposed model for long-range proton transfer is in good agreement with the experimental data obtained by other methods such as Raman spectroscopy,[15] microwave relaxation[16] and nuclear magnetic resonance spectroscopy (1D NMR,[17] 2D NMR[18]). Hayashi et al. reported that the proton transfer between two SO_4 tetrahedra is fast enough, and that the proton transfer is limited in the second stage.[19]

On the other hand, Baranowski et al. studied the pressure dependence of the phase transition and reported that the temperature of the phase transition (around 144 °C) increased linearly up to about 0.55 GPa.[20] Kreuer et al. discussed the proton transfer in the "hydrogen bond networks" of solid $CsHSO_4$ and compared this with liquid H_2O.[21] In 2001, Haile et al. first reported the applicable fuel cell properties of $CsHSO_4$ (open circuit voltage of 1.11 V and current density of 44 mA cm^{-2} when operated at 150−160 °C).[22]

Although these solid acids show high proton conductivity under non-humidified conditions, their large conductivity drops when going from superprotonic to low-temperature phases are a crucial aspect. This has prompted an interest in developing solid acid composite electrolytes with high proton conductivity over wide temperature ranges. Ponomareva et al. showed that a nearly linear Arrhenius-type proton conductivity dependence exists for $CsHSO_4$ and SiO_2 or TiO_2 composite electrolytes.[23,24] In the low-temperature phase, the composite electrolytes exhibited 2−3 orders of magnitude higher conductivity than that for pure $CsHSO_4$. However, proton conductivity in the superprotonic phase decreases by the mixing of inorganic particles.

We have previously studied the non-humidified proton conductivity of $CsHSO_4$ and phosphotungstic acid ($H_3PW_{12}O_{40}\cdot 6H_2O$: WPA-$6H_2O$) composites prepared by a mechanical milling (MM) method.[25−27] We recently reported on the non-humidified proton conductivities of $x CsHSO_4\cdot(100 - x)$WPA-$6H_2O$ (mol %) composites. Unlike $CsHSO_4$ and SiO_2 or TiO_2 composites, the $90CsHSO_4\cdot 10$WPA-$6H_2O$ composite showed a high proton conductivity of approximately 10^{-2}−10^{-4} S/cm over a wide temperature range from 160 to 30 °C. Furthermore, ^{1}H NMR measurements revealed that a new hydrogen bond was generated by mixing $CsHSO_4$ and WPA-$6H_2O$.[25]

At temperatures lower than the *Tg* of pure $CsHSO_4$, for example, 100 °C, the proton conductivities of pure $CsHSO_4$ and WPA-$6H_2O$ are 4.0×10^{-7} and 1.0×10^{-7} S/cm, respectively. On the other hand, the $90CsHSO_4\cdot$ 10WPA composite showed a much higher proton conductivity of 3.3×10^{-3} S/cm at that temperature. This strongly suggests that "*a high proton conducting reacted region*" is formed by mixing $CsHSO_4$ and WPA-$6H_2O$.

In this paper, we discuss the proton dynamics of the nanometer scale $CsHSO_4$ and WPA-$6H_2O$ reacted region and their relation to non-humidified conductivity. Proton motion at various temperatures was monitored by the ^{1}H NMR spin−lattice relaxation time (T_1). The proton conductivity of the $x CsHSO_4\cdot(100 - x)$WPA-$6H_2O$ (mol %) composites under dry conditions are also discussed based on the effective medium theory[28] to clarify the proton conductivity of the *reacted region*.

2. Experimental Section

Reagent-grade $CsHSO_4$ and $H_3PW_{12}O_{40}\cdot nH_2O$ (Wako Pure Chemical Industries) were used as starting materials. Before the mechanical milling, $H_3PW_{12}O_{40}\cdot nH_2O$ was kept at 60 °C for 6 h under an ambient atmosphere to obtain $H_3PW_{12}O_{40}\cdot 6H_2O$ (WPA-$6H_2O$). Composites of $x CsHSO_4\cdot(100 - x)$WPA-$6H_2O$ (x = 50, 60, 70, 80, 90, 95 mol %) were prepared using mechanical milling (MM). A mixture of $CsHSO_4$ and WPA-$6H_2O$ was mechanically milled under nitrogen using a planetary ball mill (Fritsch Pulverisette 7) for 10 min. No structural and conductivity changes were observed when increasing the milling period from 10 up to 60 min. Agate was selected as the material for the pot and ball. The rotation speed of the milling pot and table was kept at 720 rpm with a constant rotation ratio of 1:1. The volume of the pot was 45 mL, and 10 balls of 10 mm in

(10) Hainovsky, N. G.; Pavlukhin, Y. T.; Hairetdinov, E. F. *Solid State Ionics* **1986**, *20*, 249–253.
(11) Dolinšek, J.; Blinc, R.; Novak, A.; Shuvalov, L. A. *Solid State Commun.* **1986**, *60*, 877–879.
(12) Norby, T.; Friesel, M.; Mellander, B. E. *Solid State Ionics* **1995**, *77*, 105–110.
(13) Belushkin, A. V.; Carlile, C. J.; Shuvalov, L. A. *J. Phys.: Condens. Matter* **1992**, *4*, 389–398.
(14) Münch, W.; Kreuer, K. D.; Traub, U.; Maier, J. *Solid State Ionics* **1995**, *77*, 10–14.
(15) Pham-Thi, M.; Colomban, P.; Novak, A.; Blinc, R. *J. Raman Spectrosc.* **2005**, *18*, 185–194.
(16) Colomban, P.; Badot, J. C. *Solid State Ionics* **1993**, *61*, 55–62.
(17) Dolinšek, J.; Blinc, R.; Novak, A.; Shuvalov, L. A. *Solid State Commun.* **1986**, *60*, 877–879.
(18) Lahajnar, G.; Blinc, R.; Dolinšek, J.; Arčon, D.; Slak, J. *Solid State Ionics* **1997**, *97*, 141–144.
(19) Hayashi, S.; Mizuno, M. *Solid State Ionics* **2004**, *171*, 289–293.
(20) Baranowski, B.; Friesel, M.; Lundén, A. *Phys. A* (*Amsterdam, Neth.*) **1989**, *156*, 353–363.
(21) Kreuer, K. D. *Solid State Ionics* **1997**, *94*, 55–62.
(22) Haile, S. M.; Boysen, D. A.; Chisholm, C. R. I.; Merle, R. B. *Nature* **2001**, *410*, 910–913.
(23) Ponomareva, V. G.; Uvarov, N. F.; Lavrova, G. V.; Hairetdinov, E. F. *Solid State Ionics* **1996**, *90*, 161–166.
(24) Ponomareva, V. G.; Lavrova, G. V. *Solid State Ionics* **1998**, *106*, 137–141.
(25) Daiko, Y.; Nguyen, V. H.; Yazawa, T.; Muto, H.; Sakai, M.; Matsuda, A. Solid State Ionics (in press).
(26) Matsuda, A.; Nguyen, V. H.; Daiko, Y.; Muto, H.; Sakai, M. Solid State Ionics (in press)
(27) Daiko, Y.; Takagi, H.; Katagiri, K.; Muto, H.; Sakai, M.; Matsuda, A. *Solid State Ionics* **2008**, *179*, 1174–1177.
(28) Furusawa, S.; Miyaoka, S.; Ishibashi, Y. *J. Phys. Soc. Jpn.* **1991**, *60*, 1666–1671.

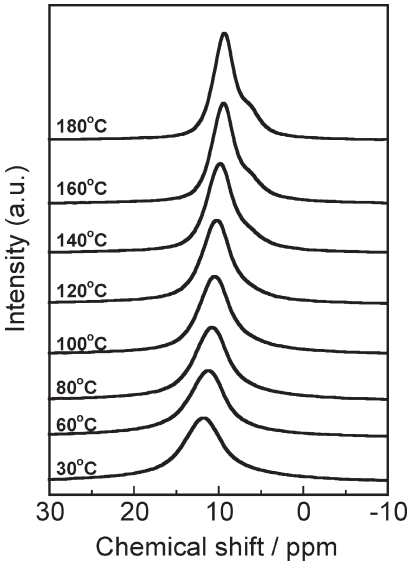

Figure 1. Temperature dependence of the ^{1}H NMR spectra of the 90CsHSO$_4$·10WPA-6H$_2$O (mol %) composite. The temperature was varied from 180 to 30 °C.

diameter were used for the mechanical milling. The sample weight was kept at 2.0 g.

The electric conductivities of the samples were determined from Cole−Cole plots obtained by an alternating current impedance method using a Solartron 1260 at frequencies ranging from 1 to 10^7 Hz. For conductivity measurements, pelletized samples (13 mm in diameter ×0.6 mm in thickness) were prepared from the composite powders by pressing under 50 MPa loading pressure. The pelletized sample was sandwiched with porous carbon paper electrodes (13 mm in diameter). The conductivity measurements were carried out under a dry nitrogen gas atmosphere.

The ^{1}H NMR spectra for static samples were measured using a Bruker ASX200 spectrometer at 200.13 MHz. A broadband probe with a solenoid coil was used. The solid echo pulse sequence ($90°_x$-τ_1-$90°_y$-τ_2-echo) was used to trace the spectra, and the latter half of the echo signal was Fourier-transformed. The 90° pulse width was 1.4 μs. The τ_1 and τ_2 values were set at 10 μs. The frequency scale of the spectra is relative to neat tetramethylsilane (TMS) by adjusting the signal of pure H$_2$O to 4.877 ppm.[29] The ^{1}H spin−lattice relaxation times were measured using Bruker Minispec mq20 and Bruker ASX200 spectrometers operating at 19.65 MHz and at 200.13 MHz, respectively. The inversion recovery pulse sequence (180° - t - 90°) was used, where t denotes the variable delay time. To remove absorbed water, the composite sample placed inside a glass tube was dried at 160 °C under vacuum for 3 h, and then the glass tube was sealed. Temperatures for the conductivity and NMR measurements were decreased from 190 to 30 °C (cooling process).

The ^{1}H magic-angle-spinning (MAS) NMR measurement was carried out at room temperature using a Bruker MSL400 spectrometer. The ordinary single pulse sequence was used. The spinning rate of the sample was 10 kHz. The frequency scale of the ^{1}H spectrum was relative to neat TMS after adjusting the signal of adamantane spinning at 8.0 kHz to 1.87 ppm.[30] Samples for the MAS NMR measurements were also dried at 160 °C under vacuum for 3 h, followed by padding into a MAS rotor under a nitrogen gas atmosphere.

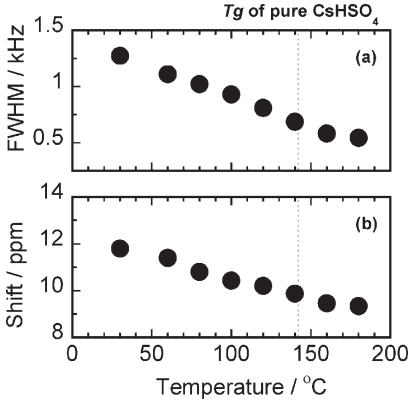

Figure 2. Temperature dependence of (a) the full width at half-maximum (fwhm) and (b) the shift in ^{1}H NMR spectra shown in Figure 1.

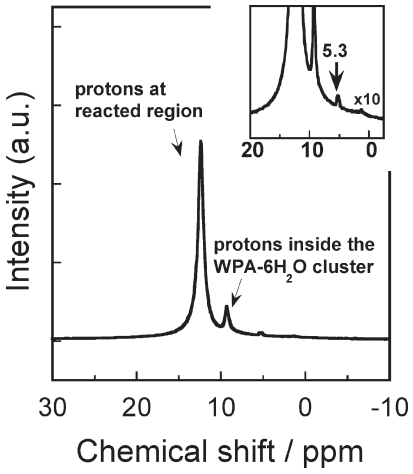

Figure 3. ^{1}H MAS NMR spectrum of the 90CsHSO$_4$·10WPA-6H$_2$O (mol %) composite measured at room temperature.

3. Results and Discussion

3.1. Protons at the Reacted Region. Changes in the ^{1}H NMR spectra (without MAS) of the 90CsHSO$_4$·10WPA-6H$_2$O (mol %) composite at various temperatures are shown in Figure 1. The line width of the spectrum at 30 °C was 1.2 kHz, and this value is much smaller than that of pure CsHSO$_4$ (~10 kHz).[31] This sharp line, which is sharp even around room temperature, is caused by mobile protons (motional narrowing). As shown in Figure 2, the line width becomes narrow, and the peak shifts to a higher magnetic field with increasing temperature. The peak shifts to higher magnetic fields, and this is related to a decrease in the hydrogen bonding strength. Note that these changes are gradual, and no significant changes in the line width and peak shift were observed around 144 °C, which is the superprotonic phase transition temperature of pure CsHSO$_4$.

When CsHSO$_4$ and WPA-6H$_2$O were mixed, an ion exchange reaction between Cs^+ and H^+ occurs.[32,33] The size of the WPA-6H$_2$O cluster inside the 90CsHSO$_4$·

(29) Hayashi, S.; Yanagisawa, M.; Hayamizu, K. *Anal. Sci.* **1991**, *7*, 955–957.
(30) Hayashi, S.; Mizuno, M. *Solid State Commun.* **2004**, *132*, 443–448.
(31) Mizuno, M.; Hayashi, S. *Solid State Ionics* **2004**, *167*, 317–323.
(32) Dias, J. A.; Caliman, E.; Dias, S. C. L. *Microporous Mesoporous Mater.* **2004**, *76*, 221–232.
(33) Molnár, Á.; Beregszászi, T.; Fudala, Á.; Lentz, P.; Nagy, J. B.; Kónya, Z.; Kiricsi, I. *J. Catal.* **2001**, *202*, 379–386.

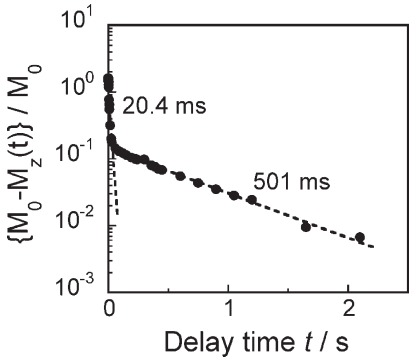

Figure 4. Magnetization recovery curve for the $90CsHSO_4 \cdot 10WPA\text{-}6H_2O$ (mol %) composite measured at 200.13 MHz and 190 °C using the inversion−recovery method.

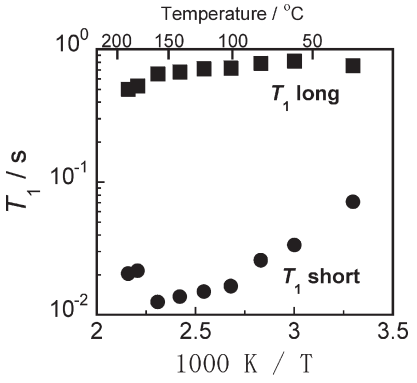

Figure 5. Temperature dependence of the shorter and longer T_1 values of the $90CsHSO_4 \cdot 10WPA\text{-}6H_2O$ (mol %) composite measured at 200.13 MHz.

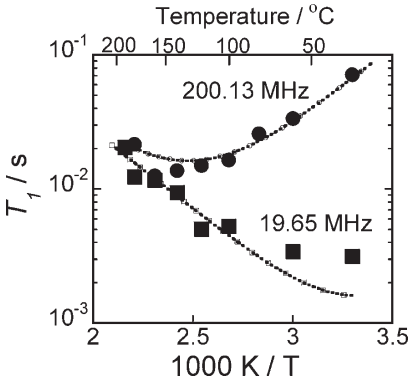

Figure 6. Temperature dependence of the shorter T_1 of the $90CsHSO_4 \cdot 10WPA\text{-}6H_2O$ (mol %) composite measured at 19.65 and 200.13 MHz. The dotted lines are the fitting results calculated using eqs 2 and 3.

$10WPA\text{-}6H_2O$ (mol %) composite was roughly estimated to be 30 nm from the X-ray diffraction (XRD) pattern using Scherrer's equation. Cs^+ ions were inserted into the $WPA\text{-}6H_2O$ cluster, and the proton concentration around the cluster should increase after the ion exchange reaction. Figure 3 shows the ^1H MAS NMR spectrum of the $90CsHSO_4 \cdot 10WPA\text{-}6H_2O$ (mol %) composite measured at room temperature. Two peaks are clear at 12.4 and 9.3 ppm. The amounts of protons were estimated to be 93% (12.4 ppm) and 7% (9.3 ppm), respectively, from the integral intensities of each peak. A very small peak is observed at 5.3 ppm with less than 1% of the total intensity, which is ascribed to water adsorbed on the external surface. The separate observation of this peak indicates that the adsorbed water does not exchange with other types of protons. Consequently, this water does not contribute to proton conduction or T_1 results described below. From the integral intensities, we attributed the peaks at 12.4 and 9.3 ppm to protons from the $CsHSO_4$/$WPA\text{-}6H_2O$ reacted region and those from the $WPA\text{-}6H_2O$ clusters, respectively. Protons inside the $WPA\text{-}6H_2O$ cluster did not exchange with Cs^+ ions.

The inversion recovery method was used to determine the spin−lattice relaxation time, T_1. The magnetization recovery was measured at 200.13 MHz and is plotted in Figure 4 as a function of the delay time t. It is clear that there are two relaxation components. Similar relaxation behavior was also observed using the Bruker Minispec mq20 spectrometer (operated at 19.65 MHz). The spin−lattice relaxation is a first order kinetic process:

$$\{M_0 - M_z(t)\}/M_0 = A \exp(-t/T_1) \qquad (1)$$

where $M_z(t)$ is the magnetization at time t, M_0 is the magnetization at equilibrium, and A is a fitting parameter. From eq 1, the short and long T_1 values were calculated to be 20.4 and 501 ms, respectively. The amount of protons with the shorter T_1, which can also be estimated from the magnetization intensities in Figure 4, was approximately 95% of all the protons.

Figure 5 shows the temperature dependence of the long and short T_1 measured at 200.13 MHz. A typical V-shaped change (Bloembergen, Purcell, and Pound, BPP dependence[34,35]) was observed for the shorter T_1 whereas the longer T_1 values decreased gradually with increasing temperature. It is evident from these temperature dependencies that the motion of protons that have a longer T_1 is much slower than that of the protons with the shorter T_1.

In the medium temperature region, for example, 100 °C under dry conditions, as mentioned above, $WPA\text{-}6H_2O$ shows a very low proton conductivity of 1.0×10^{-7} S/cm with an activation energy of ~100 kJ/mol.[36] Protons inside the $WPA\text{-}6H_2O$ cluster were not mobile under non-humidified conditions. On the other hand, the composite ($x = 90$) showed a proton conductivity of 3.3×10^{-3} S/cm at this temperature. From the MAS NMR (the amount of protons), the T_1 values as well as proton conductivity results, we conclude that the protons with the shorter T_1 are in the $CsHSO_4$ and $WPA\text{-}6H_2O$ reacted region, and those with the longer T_1 are in the $WPA\text{-}6H_2O$ cluster.

3.2. Analysis of the Shorter Spin−Lattice Relaxation Time. The short T_1 values measured at 19.65 and 200.13 MHz are plotted in Figure 6 as a function of the reciprocal

(34) Bloenbergen, N.; Purcell, E. M.; Pound, R. V. *Phys. Rev.* **1948**, *73*, 679–712.
(35) Abragam, A. *The Principles of Nuclear Magnetism*; Oxford Univ. Press: London, 1961.
(36) Janik, M. J.; Davis, R. J.; Neurock, M. *J. Am. Chem. Soc.* **1992**, *127*, 5238–5245.

Table 1. Activation Energies, the Mean Residence Times at the Infinite Temperature, and the Second Moments for the 90$CsHSO_4$·10WPA-6H_2O (mol %) Composite and Pure $CsHSO_4$[a]

sample	ΔE/kJ mol^{-1}	τ_0/s	M_{HH}/kHz^2
x = 90 composite	22.5	7.5×10^{-12}	330
$CsHSO_4$[b] (superprotonic phase)	35	1.7×10^{-13}	6.5

[a] Calculated from the structure of the superprotonic phase. [b] Reference no. 19.

temperature. The temperature and frequency dependences of the T_1 values were analyzed theoretically according to BPP theory.[34,35] Relaxation by dipolar interaction is the most probable mechanism in the present system, and the dipolar contribution to the spin−lattice relaxation can be written as[19]

$$(T_1)^{-1} = \frac{2}{3} M_{HH} \left[\frac{0.5\tau_H}{1+(0.5\omega_H\tau_H)^2} + \frac{2\tau_H}{1+(\omega_H\tau_H)^2} \right] \quad (2)$$

where ω_H is the angular resonance frequency of a ^1H nucleus, M_{HH} is the second moment due to the $^1H-^1H$ dipole−dipole interaction, and τ_H is the mean residence time of protons. τ_H is a function of temperature and is assumed to follow the Arrhenius relation as

$$\tau_H = \tau_0 \exp(\Delta E/RT) \quad (3)$$

where τ_0 is the mean residence time at infinite temperature, ΔE is the activation energy for a proton jump in the nanometer scale, R is the gas constant, and T is the temperature. The T_1 values were fitted using eqs 2 and 3, shown in Figure 6 as dotted lines. The fitting parameters were M_{HH}, τ_0, and ΔE. The obtained values are summarized in Table 1 with the results from pure $CsHSO_4$. Note that the 90$CsHSO_4$·10WPA-6H_2O composite has a far lower ΔE of 22 kJ/mol than that of pure $CsHSO_4$ (in the superprotonic phase, 35 kJ/mol). In the *reacted region*, the barrier for the proton jump in the nanometer scale decreased significantly.

Figure 7 shows the temperature dependence of the τ_H values for the 90$CsHSO_4$·10WPA-6H_2O composite and pure $CsHSO_4$.[19,30] For comparison, the τ_H values at 100 °C for the composite and pure $CsHSO_4$ are 1.07×10^{-8} and 1.7×10^{-5} s, respectively. Note that the τ_H value decreases by more than 3 orders of magnitude owing to the complexation. This means that the rate of proton jumping under dry conditions is about 1,600 times higher after the addition of 10 mol % WPA-6H_2O.

The mean residence time τ_H calculated from the shorter T_1 values, which is related to the proton dynamics in the reacted region, was used to estimate the macroscopic proton conductivity. Diffusion constants can be calculated from τ_H by the following equation:

$$D = \frac{L^2}{n\tau_H} \quad (4)$$

where L is the jumping distance and n is the number of sites to which H can jump (n is assumed to be 6 because of three-dimensional diffusion). For pure $CsHSO_4$, L was calculated to be 0.46 nm from the crystal structure. Here, we estimate L for the 90$CsHSO_4$·10WPA-6H_2O composite using the M_{HH} values:

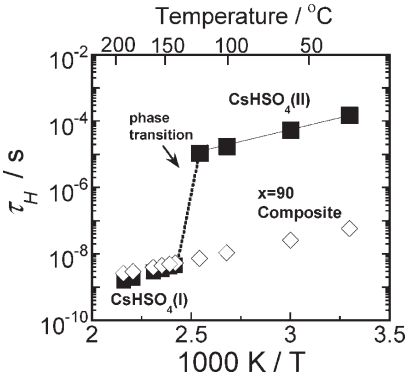

Figure 7. Temperature dependence of the mean residence time τ_H of pure $CsHSO_4$ and the 90$CsHSO_4$·10WPA-6H_2O (mol %) composite.

$$M_{HH} = \frac{3}{5}\gamma_H^4\hbar^2 I_H(I_H+1)\sum_i r_i^{-6} \quad (5)$$

where γ_H is the gyromagnetic ratio, $\hbar$ is the Plank constant, and I_H is the nuclear spin quantum number (I_H = 1/2). The distance between ^1H spins is denoted as r_i, which directly correlates to the jumping distance L in eq 4. From the M_{HH} values, the corresponding L for the x = 90 composite was estimated to be 0.23 nm. A diffusion constant of 8.2×10^{-13} m^2/s was thus obtained for the x = 90 composite at 100 °C.

The electrical conductivity (σ) is related to the proton diffusion constant by the following equation:

$$\sigma = Ne^2D/kT \quad (6)$$

where N is the density of mobile protons, e is the proton charge, and k is the Boltzmann constant. The N of pure $CsHSO_4$ (superprotonic phase) was calculated to be 8.48×10^{27} m^{-3} from the crystal structure. Considering a simple lattice with two protons in the unit cell, the N value increases approximately 8-fold when L changes from 0.43 to 0.23 nm. From the NMR analysis using eqs 4−6, the proton conductivity at 100 °C of the reacted region was estimated to be 2.8×10^{-3} S/cm. Note that the estimated proton conductivity was in good agreement with the bulk proton conductivity measured by the impedance method (3.3×10^{-3} S/cm). The proton conductivity of the *reacted region* is predominantly determined by the motion of protons with the shorter T_1, and protons with longer T_1 do not contribute to the long-range proton diffusion (conductivity) under dry conditions.

As shown in Table 1, the composite shows larger second moment of 330 kHz^2 than pure $CsHSO_4$ (6.5 kHz^2). The M_{HH} value relates the proton concentration, and results also suggest the higher proton concentration of the 90$CsHSO_4$·10WPA-6H_2O (mol %) composite compared with pure $CsHSO_4$. Also, the jumping distance L of the composite is smaller than that of pure $CsHSO_4$.

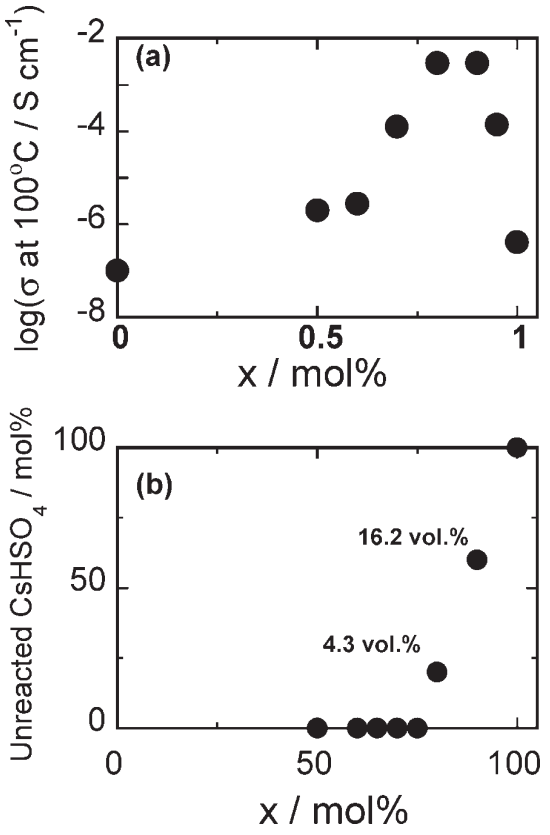

Figure 8. (a) Proton conductivity and (b) the amount of the unreacted residual $CsHSO_4$ with composition x.

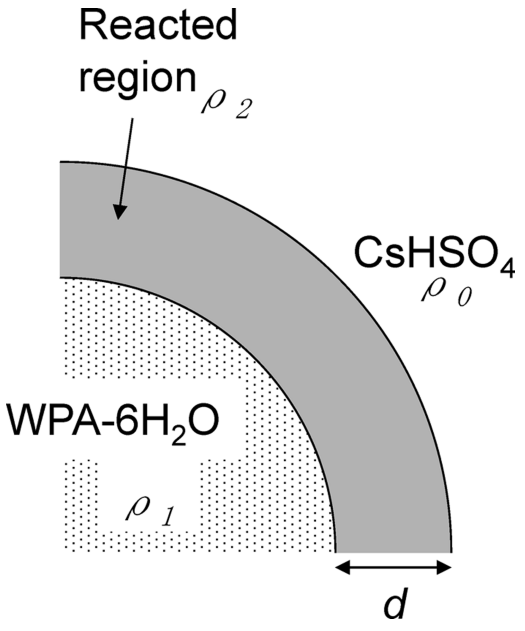

Figure 9. Schematic of the calculation model used for the $CsHSO_4$·WPA-$6H_2O$ composites.

From these M_{HH} and L values, the decrease of the activation energy from 35 to 22.5 kJ/mol is considered to be related with both the increase of proton concentration and the decrease of the jumping distance.

3.3. Effective Medium Theory. Nanometer scale proton motion under dry conditions was enhanced significantly by mixing 10 mol % WPA-$6H_2O$. Using the

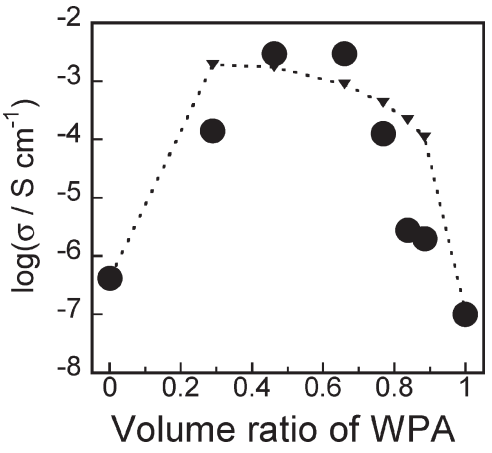

Figure 10. Proton conductivity of the composites (●) shown in Figure 8(a) as a function of the volume ratio of WPA. The dotted line is the fitting result calculated using eqs 9a−12.

conductivity data of composites with various compositions as well as pure $CsHSO_4$ and WPA-$6H_2O$, the formation of the "*high proton conducting reacted region*" and its proton conductivity are also discussed. The proton conductivities of composites were theoretically calculated by the effective medium theory.[28] The effective medium theory used is based on a percolation model.

Figure 8a shows the proton conductivity at 100 °C of the compositions x. The proton conductivity of the $CsHSO_4$·WPA-$6H_2O$ composites increases clearly from $x = 60$. By increasing the x value, the reacted region percolates, and proton conductivity increases significantly after the percolation.

When $CsHSO_4$ reacts with WPA-$6H_2O$, the following ion exchange reaction occurs[32,33] and above $x = 75$, a part of the $CsHSO_4$ remains unchanged. For example,

$$(x = 50)\quad 50CsHSO_4 + 50H_3PW_{12}O_{40}\text{-}6H_2O \rightarrow 50CsH_2PW_{12}O_{40}\text{-}6H_2O + 50H_2SO_4 \qquad (7)$$

$$(x = 95)\quad 95CsHSO_4 + 5H_3PW_{12}O_{40}\text{-}6H_2O \rightarrow 5Cs_3PW_{12}O_{40}\text{-}6H_2O + 15H_2SO_4 + 80CsHSO_4 \qquad (8)$$

We measured the ^{31}P MAS NMR spectrum of the $x = 90$ composite to confirm the ion exchange reaction. A signal attributed to $Cs_3PW_{12}O_{40}$[32] was mainly observed at −14.8 ppm (spectra are not shown). The unreacted residual $CsHSO_4$ phase was also verified by X-ray diffraction of the $x = 95$ composite. The calculated amount of residual $CsHSO_4$ is plotted in Figure 8b for the compositions x. Because of the very low proton conductivity of pure $CsHSO_4$ at 100 °C, the conductivity decreased markedly above $x = 90$ where the amount of unreacted residual $CsHSO_4$ was 16.2 vol %. Direct evidence for the formation of liquid H_2SO_4 after the ion exchange reaction was not obtained.

We considered the calculation model shown in Figure 9 where $CsHSO_4$ as a matrix with an electric resistance ρ_0 (Ω·cm) is replaced randomly with WPA (the resistance ρ_1

and the volume ratio p). A high proton conducting reacted region with thickness d and resistance ρ_2 forms around the WPA clusters. The subscript numbers 0, 1, and 2 represents the matrix ($CsHSO_4$), additive (WPA), and reacted regions, respectively. Here, we assumed that the resistance of the reacted region does not change as the composition x changes (ρ_2 is constant). The probabilities P_i ($i = 0, 1, 2$ and $P_0 + P_1 + P_2 = 1$), which are a function of the volume fraction p, are given as

$$P_0 = (1-p)^m \tag{9a}$$

$$P_1 = p \tag{9b}$$

$$P_2 = (1-p)[1-(1-p)^{m-1}] \tag{9c}$$

$$m = (d/a)^3 \tag{9d}$$

Here, a in eq 9d is an arbitrarily introduced characteristic length.[28] According to the calculation by Furusawa et al., the mean bulk resistance ρ^* can be represented as follows:

$$\frac{(1-\rho_0)-(1/\rho^*)}{(1/\rho_0)+(2/\rho^*)}P_0 + \frac{(1/\rho_r)-(1/\rho^*)}{(1/\rho_r)+(2/\rho^*)}(P_1+P_2) = 0 \tag{10}$$

where ρ_r is related to the resistances of both the added WPA (ρ_1) and the reacted region (ρ_2).

$$\frac{1}{\rho_r} = \frac{1}{\rho_1+(c-1)\rho_2} + \frac{1}{[c/(c-1)]\rho_2} \tag{11}$$

$$c = \sqrt{1+(1-p)^2} \tag{12}$$

The experimentally obtained proton conductivities shown in Figure 8a were fitted using eqs 9a−12. The fitting parameters were the resistance of the reacted region ρ_2 and m of eq 9d. The experimentally obtained proton conductivities are replotted in Figure 10 as a function of the volume ratio of the added WPA (p). The simulated proton conductivities ($1/\rho^*$) are also shown in Figure 10 as a dotted line. The obtained proton conductivity of the reacted region and the parameter m were 10×10^{-3} S/cm and $m = 5.46$, respectively. Note that the theoretically calculated proton conductivity of the reacted region is in good agreement with that calculated from the analysis of the shorter T_1 (2.8×10^{-3} S/cm). It is evident from these calculations (NMR and effective medium theory) and impedance results that reacted regions with high proton conductivity under dry conditions can be formed around the added WPA.

WPA has three protons, and the proton concentration in the reacted region should increase because of the ion exchange reaction $Cs^+ \leftrightarrow H^+$. This results in the formation of a hydrogen bonding reacted region around WPA-$6H_2O$ with very high proton conductivities even under dry conditions. A schematic illustration of the reacted region is shown in Figure 11. An appropriate amount of WPA-$6H_2O$ is, therefore, effective in significantly improving the non-humidified proton conductivity. However, it should be noted that in Figure 10 approximately

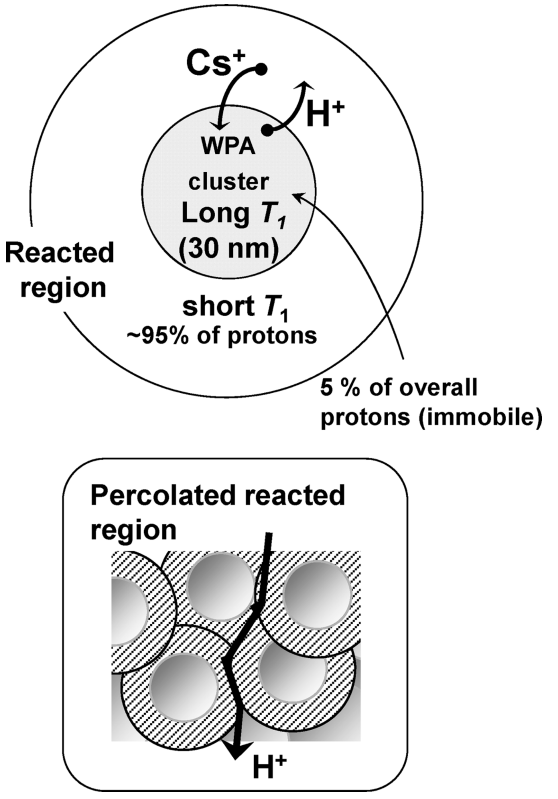

Figure 11. Schematic illustration of the reacted region for the $CsHSO_4 \cdot$WPA-$6H_2O$ composites.

2 orders of magnitude difference is apparent between the experimental data and the simulated conductivity at around 0.8 WPA volume ratio. The assumption that ρ_2 is constant may cause these differences, and further studies about the hydrogen bonding network, non-humidified proton conductivity for various types of proton conductors, and long-term stabilities of the composite are in progress to understand the non-humidified proton conduction mechanism.

4. Conclusions

$CsHSO_4$ and WPA-$6H_2O$ composites were prepared by mechanical milling. The proton dynamics and the non-humidified proton conductivity were investigated. The proton conductivity under dry conditions increased significantly by mixing $CsHSO_4$ and WPA-$6H_2O$. Two types of relaxation (longer T_1 and shorter T_1) were clearly observed by spin−lattice relaxation measurements. We concluded that protons with a longer T_1 are in the WPA-$6H_2O$ cluster and those with a shorter T_1 are in the $CsHSO_4$ and WPA-$6H_2O$ *reacted region*. The barrier energy of proton hopping from one site to a neighboring one decreased from 35 to 22 kJ/mol by complexation. The hopping frequency at 100 °C of the $90CsHSO_4 \cdot 10$WPA-$6H_2O$ (mol %) composite was about 1,600 times higher than that of pure $CsHSO_4$. The proton conductivity at 100 °C of the $90CsHSO_4 \cdot 10$W-PA-$6H_2O$ (mol %) reacted region was 3.3×10^{-3} S/cm. Similar proton conductivity for the $x = 90$ composite (2.8×10^{-3} S/cm) was obtained from the NMR results of

protons with a shorter T_1, suggesting that the protons with a shorter T_1 have a dominant contribution to the long-range proton diffusion under dry conditions, while those with a longer T_1 do not. Furthermore, from the proton conductivities of the composites with various compositions, the proton conductivity of the reacted region was theoretically calculated to be approximately 10×10^{-3} S/cm, which is in good agreement with impedance and NMR results. A reacted region with a high proton conductivity under dry conditions can form around the WPA-$6H_2O$ cluster through an ion exchange reaction between the H^+ of WPA-$6H_2O$ and the Cs^+ of $CsHSO_4$. The proton conductivity of the composite increased significantly after percolation of the reacted region.

Acknowledgment. This work was supported by the Ministry of Education, Culture, Sports, Science, and Technology of Japan (Grant-in-Aid for Scientific Research on Priority Areas No.439 "Nanoionics," A02 No.19017009), by the Japan Society for the Promotion of Science (Challenging Exploratory Research No.21655075.) and by the Murata Science Foundation.